energies

MDPI

Article

Prony Method Estimation for Motor Current Signal Analysis Diagnostics in Rotor Cage Induction Motors

Luis Alonso Trujillo Guajardo *, Miguel Angel Platas Garza, Johnny Rodríguez Maldonado, Mario Alberto González Vázquez, Luis Humberto Rodríguez Alfaro and Fernando Salinas Salinas

Universidad Autónoma de Nuevo León, UANL, FIME, Av. Universidad S/N Ciudad Universitaria, San Nicolás de los Garza C.P. 66451, NL, Mexico; miguel.platasgrz@uanl.edu.mx (M.A.P.G.); johnny.rodriguezml@uanl.edu.mx (J.R.M.); mario.gonzalezvzq@uanl.edu.mx (M.A.G.V.); luis.rodriguezlf@uanl.edu.mx (L.H.R.A.); fernando.salinassln@uanl.edu.mx (F.S.S.)
* Correspondence: luis.trujillogjr@uanl.edu.mx; Tel.: +52-818-329-4020

Abstract: This article presents an evaluation of Prony method and its implementation considerations for motor current signal analysis diagnostics in rotor cage induction motors. The broken rotor bar fault signature in current signals is evaluated using Prony method, where its advantages in comparison with fast Fourier transform are presented. The broken rotor bar fault signature could occur during the life cycle operation of induction motors, so that is why an effective early detection estimation technique of this fault could prevent an insulation failure or heavy damage, leaving the motor out of service. First, an overview of cage winding defects in rotor cage induction motors is presented. Next, Prony method and its considerations for the implementation in current signature analysis are described. Then, the performance of Prony method using numerical simulations is evaluated. Lastly, an assessment of Prony method as a tool for current signal analysis diagnostics is performed using a laboratory test system where real signals of an induction motor with broken rotor bar operated with/without a variable frequency drive are analyzed. The summary results of the estimation (amplitudes and frequencies) are presented in the results and discussion section.

Keywords: Prony method; broken rotor bar; fast Fourier transform; current signal analysis

check for updates

Citation: Trujillo Guajardo, L.A.; Platas Garza, M.A.; Rodríguez Maldonado, J.; González Vázquez, M.A.; Rodríguez Alfaro, L.H.; Salinas Salinas, F. Prony Method Estimation for Motor Current Signal Analysis Diagnostics in Rotor Cage Induction Motors. *Energies* **2022**, *15*, 3513. https://doi.org/10.3390/en15103513

Academic Editors: Daniel Morinigo-Sotelo, Rene Romero-Troncoso and Joan Pons-Llinares

Received: 18 March 2022
Accepted: 9 May 2022
Published: 11 May 2022

Publisher's Note: MDPI stays neutral with regard to jurisdictional claims in published maps and institutional affiliations.

Copyright: © 2022 by the authors. Licensee MDPI, Basel, Switzerland. This article is an open access article distributed under the terms and conditions of the Creative Commons Attribution (CC BY) license (https://creativecommons.org/licenses/by/4.0/).

1. Introduction

Electric motors, particularly rotor cage induction motors (RCIM) are considered for most of industry applications, because of its operation performance and low maintenance cost. According to statistical studies performed by IEEE and Electric Power Research Institute, a percentage of 8–9% of the total RCIM faults occur in the rotor [1], where broken rotor bars (BRB) or cracked/broken end rings (CBER) are the most common issues in RCIM operation. It is well-known that the cage of RCIM is made typically of aluminum and in some cases of copper [2]. BRB or CBER will have a high probability of appearing when, for example a RCIM is operated considering several direct-on-line (DOL) starts in a short period of time or RCIM with high inertial loads, these conditions will put the RCIM through an excessive centrifugal, thermal, and mechanical stress. It is important to mention that a BRB or CBER cause a reduction in RCIM operation performance, for example, having problems to move its load mainly due to an unbalanced flux in the rotor causing a reduction in the output torque [3] and heavy damage to the RCIM. So, to prevent a heavy damage situation, BRB or CBER must be detected early in a noninvasive way, where as a part of condition monitoring of RCIM, motor current signature analysis (MCSA) is used to determine problems such as BRB, CBER, or abnormal air gap eccentricity (AAGE) at the rotor cage when the motor is under normal operation.

It is important that BRB or CBER are accurately detected using MCSA. However, in some cases there exist "false positives", which means an unnecessary shut down and transportation to a qualified repair facility, and if the RCIM is a large machine there will

be higher costs from loss in production and maintenance expenses than the cost of a new motor [4]. On the other hand, if there is a "false negative" the motor will be kept in operation and a catastrophic failure will occur if the broken rotor bar reaches the stator winding.

Recently, in the last three years, research has been going on to detect RCIM and BRB faults in a noninvasive way and several methods and techniques have been presented in the literature. For example in [5], an analysis using a new algorithm based on the Park's transformation, where the direct and quadrature current components were analyzed for BRB fault detection and identification; in [6], finite element software is proposed to be used to detect motor broken bar mechanical fault by detecting magnetic flux density fluctuations; in [7], a novel methodology based on motor current signal analysis and contrast estimation is introduced for BRB detection, where a textural feature "Contrast" commonly used for image classification in combination with fuzzy logic classifier is proposed for BRB detection; in [8], an intelligent multi-agentsystem (MAS) is proposed to make decisions on the fault conditioning of a three-phase squirrel cage induction motor where also artificial intelligent methods are used; in [9], a two-stage approach for three-phase induction motors diagnosis based on mutual information measures of the current signals, principal component analysis, and intelligent systems is proposed; in [10], an approach based on the analysis of the startup transient current signal through the current signal homogeneity and the fourth central moment (kurtosis) analysis is presented, where these features are used for training a feed-forward, backpropagation artificial neural network used as a classifier; in [11] a scheme to detect broken bar faults and discriminate the severity of faults under starting conditions is presented, where a successive variable mode decomposition (SVMD) is applied to analyze the stator starting current to extract the fault component, and the signal reconstruction is proposed to maximize the energy of the fault component, and so the signature frequency could be detected; in [12], an end-ring wear detection through a multicomponent approach is researched; in [13], an estimate of the fundamental frequency component from an optimization point of view is proposed; in [14], magnetic flux condition monitoring is reviewed in detail, and it is focused on the diagnosis of different types of faults in the most common rotating electric machines used in industry; in [15–19], several methods focus on RCIM using variable frequency drives where the proposed methods have in common start up transient analysis, and others considers bar breakage harmonics evolution for BRB diagnostics; finally, in [20], a zero-setting protection element, which uses the current signature method is proposed to detect broken rotor bars, where the research has been applied in commercial protection relay equipment, and considers the use of an alpha current signal to obtain the frequency spectrum of the signal to detect the BRB fault signature. Nevertheless, MCSA as condition monitoring has been popular to help diagnose RCIM problems since the 1970s and it is commonly used in online test equipment because it only needs voltage and current probes. In online test equipment for RCIM, the tester records voltage and current signals with a defined resolution and observation window which is selected prior to perform a test. Data acquisition is enabled so that the tester software can record the signals and spectral analysis using fast Fourier transform (FFT) [21] can be performed. It should be mentioned that FFT is the widely used digital signal processing technique for this application, where fault signature frequencies can be detected, and a diagnostic can be issued [22]. However, FFT has some limitations that could lead to misdiagnosis of BRB: If the tester user performs the measurement without knowing in detail the different conditions or situations in which a misdiagnosis of BRB can occur, for these scenarios if a load variation during the acquisition of signals occur, if the machine is under low load conditions, or if a short sampling time or length of the recorded signal is not adequate (too short) the spectral analysis of the measured signal will estimate frequencies that are not really there, or simply the BRB fault signature frequencies will not be detected [23]. This is why it is important to mention that knowing how the data acquisition and recording is performed in order to find the limitations is highly recommended, for the main purpose of being able to have an accurate diagnosis, whether there is a BRB fault or not. The reader should know that rotor cage faults such as BRB or

CBER produce a magnetic asymmetry in the air gap, and the asymmetry will be adding specific frequencies which are close to the fundamental frequency that will be appearing at motor line current measurement.

Different techniques for BRB detection have been studied in the last 10 years, for example [5–19,23–28], where some of these techniques require fixed observation windows and others considers recursive algorithms, artificially intelligent methods, startup transient analysis, and new developed transforms such as the dragon transform, these techniques that were studied and proposed for BRB fault signature detection have one point in common, which is the complexity of the practical implementation due to its considerations and calculations, nevertheless, none of these techniques are used nowadays in commercial online test diagnostics (OTD) equipment, the estimation technique used is a FFT-based tool which has its estimation limitations. To overcome the limitations of the FFT-based tool, in this work, the parametric estimation technique Prony method has been proposed as a BRB detection technique to increase the accuracy of the detection of rotor cage fault signature frequencies, particularly BRB sideband frequencies. In the recent years, only five articles have considered the Prony method for BRB fault detection [29–33]. For example, [29] considered using the Prony method to estimate frequency and amplitudes of a signal under analysis using different windows length of recorded data samples. [30] proposed the use of Prony method with other technique, such as Hilbert transform and discrete wavelet transform. In [31], the Prony method was used to evaluate different load conditions at a defined sampling frequency. [32] proposed the use of Prony method in combination with singular value decomposition (SVD) filtering technique and Multiple Signal Classification (MUSIC). [33] proposed the use of a modified Prony method in combination with MUSIC algorithm. In [29,31], the Prony method is used for BRB diagnosis and an analysis of different lengths of data at different load conditions is presented, however, no analysis and validation considering VFD is reported which is a common industry application. In this work, in order to fulfill the application considerations and validation that where not considered in the mentioned references, relevant and application details described in Sections 3 and 4 are presented, where also VFD operation at different speeds for full load condition is evaluated to guarantee an accurate detection of BRB and a diagnosis of the cage of the rotor can be accurately determined.

In this investigation, numerical simulated signal and a laboratory test system with a faulted RCIM being operated and controlled by a VFD under different speed conditions is considered for the validation of the method for its practical application for detection of cage rotor faults, and a comparison with FFT analysis is also considered to show the limitations of using FFT for this particular application. In this approach, the considerations required for the application of Prony method for an accurate detection of cage rotor fault signature frequencies and its magnitudes are described. First, a fixed window of data samples is defined. Then, the signal under analysis is digitally processed and downsampled. Moreover, a low pass and DC filter is applied to the downsampled signal, where the processed output signal is the input signal for Prony method estimation algorithm. The purpose of subsampling is to reduce the computational calculation of the algorithm, because commercial equipment for OTD considers a defined high sampling frequency, which is not needed to estimate the low frequencies related with the rotor fault; also a low pass and DC filter stage is needed to eliminate undesired frequencies in the signal, and to reduce the noise of the signal to the minimum, so an accurate estimate of the amplitudes and frequencies of the BRB signature components can be achieved.

The paper is organized as follows. First, an overview of diagnostics on cage winding defects is described in Section 2. The Prony method and its application considerations are discussed in Section 3. Then, a study case considering numerical simulated signals and a laboratory test system for MCSA where numerical and experimental results comparison between FFT analysis and Prony method estimation are presented in Section 4. Finally, a summary of the results achieved is presented in Section 5, where the performance of Prony method for this application is also discussed.

The main contribution of this article is that Prony method can be considered as a diagnostic tool in BRB OTD, where its application could be feasible, and with lesser recorded data signal values, in comparison with FFT analysis, a good estimate of sideband frequencies and its amplitudes can be obtained, the method can be used as a new tool to improve the accuracy and sensitivity of OTD in RCIM, and it could be implemented in the existing or new software in online test equipment's for electric motors with no need of hardware updates. The methodology was validated by using simulation signals and real data signals, and its effectiveness is presented.

2. Overview of Diagnostics on Cage Winding Defects

In this section, fundamental aspects of broken rotor bar side band frequencies (BRB_{sbf}) required for the detection of these components during the estimation of a current signal under analysis are presented. When a RCIM has a fracture or break in its cage (BRB or CBER), see Figure 1, the effects within the motor result in voltages at specific frequencies as presented in Equation (1), mainly due to the alteration of the magnetic field at the cage of the rotor.

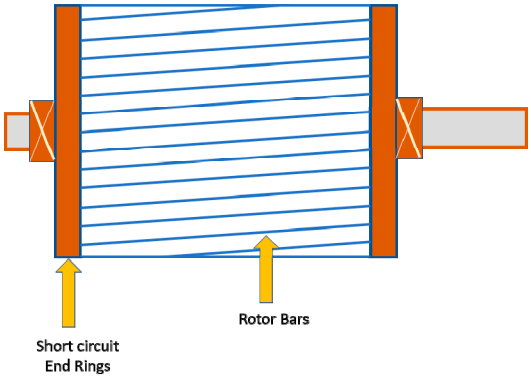

Figure 1. Illustration of a caged rotor of a RCIM.

BRB and CBER in a RCIM are mainly caused due to a maloperation, such as, too many sequential direct on-line starts where time delay between starts is not adequate according to manufacturer specification, which causes high starting currents, also, an incorrect match of torque-speed curve of RCIM and torque-speed curve of the load. These operation conditions add excessive centrifugal, mechanical, and thermal stress at the slip ring which can result in a BRB or CBER fault. Due to a BRB or CBER, an unbalanced rotor flux occurs and an effect in motor operation performance appears, for example, line currents oscillation, torque pulsation, decreased average torque, and excessive vibration [3,4]. If the BRB or CBER fault are not detected, an insulation failure or heavy damage could occur, and a replacement of the RCIM will be required.

The BRB_{sbf} in a RCIM considers the supply fundamental frequency (f_0), the slip of the motor (s), and its harmonic value (h), which represent the number of broken rotor bars that could appear in the RCIM [3,4]. The equation for BRB_{sbf} in a RCIM is presented in Equation (1):

$$BRB_{sbf} = f_0(1 \pm 2 * h * s) \quad (1)$$

The BRB_{sbf} affects the RCIM operation if the energy of the frequencies is within the fault indication value of a break in the cage rotor circuit; typical failure signature values considered are presented in Table 1.

Some physical conditions affect the magnitude of BRB_{sbf}, which can affect the resulting diagnostic during a MCSA. Some of these conditions are, change in load and slip with a fixed rotor cage defect, faulty bar to end ring joints creating an asymmetrical cage, porosity and consequential arcing in aluminum die-cast cage rotors, partially broken rotor bars, actual broken bars still making contact with an end ring and bars which are cracked from the top of the bar, but just a percentage of the total depth of the bar [4]. It is important to

mention that it is not possible to predict exact severity of cage defects/number of BRB or CBER from the magnitudes in dB of the BRB_{sbf} with respect to f_0, only an estimate of the condition of the cage winding can be defined as presented in Table 1.

Table 1. Rotor condition sideband frequency failure signature.

Energy, dB	Rotor Condition
>60	Excellent
54–60	Good
48–54	Moderate
42–48	High resistance connection or cracked bars
36–42	Broken rotor bars will show in vibration analysis
30–36	Multiple $\frac{\text{cracked}}{\text{broken}}$ bars, possible ring problems
<30	Severe rotor faults

The accuracy of the estimation of magnitudes in dB of BRB_{sbf} of a motor current signal under analysis depends on the digital signal processing (DSP) technique, see Figure 2. Nowadays, modern on-line test equipment use the fast Fourier transform (FFT) spectral analysis to detect harmonics and other frequencies such as BRB_{sbf}; this is a commonly used technique but it has its limitations, for example, (a) the motor current signals measurements should be performed during steady state operation of the motor, so the estimation of frequencies and its magnitudes detected could be accurate, (b) the recorded current signal should have between 10 and 120 s of acquire data without any load variations during acquisition, in terms of signals cycles for a 60 Hz or 50 Hz, a minimum of 600 or 500 cycles of recorded signal should be required at least to be able to detect BRB_{sbf}, because these frequencies are too close to the fundamental frequency. In the case of motor operation with VFD, the number of signal cycles will be proportional to the operation frequency considering the same length between 10 and 120 s of acquired data. It should be mentioned that in case of a motor under low load or no-load operation, the cage winding circulating currents will be minimum or null, so at this condition the BRB_{sbf} cannot be detected with the estimation technique being used.

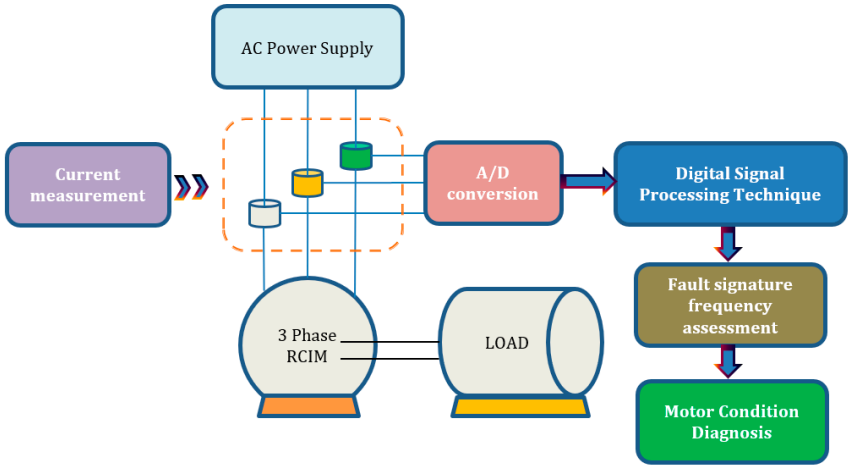

Figure 2. General scheme of MCSA for RCIM.

3. Prony Method Estimation for Motor Current Signal Analysis

Prony method is a signal processing technique based on signal estimation, which extracts desired information from an equally spaced sampled signal and builds a series of damped complex exponentials to approximate the sampled signal by solving a set of linear equations. The Prony algorithm and its practical implementation are presented

in [34,35], and have been used for power quality analysis [36–38], stability studies applied to power system and nuclear power plants [39,40], and also have been evaluated and patented for real time application in power system protection mainly in distance relay algorithms [41,42]. It should be mentioned that the Prony method is also evaluated for the detection of BRB in other works as itself or used with other technique [29–33], but not enough details are presented for its implementation, and validation analysis of the method for this application is not fulfilled. To overcome this, Prony method is proposed as an additional diagnostic algorithm to estimate the parameters of the current waveforms recorded during an OTD for RCIM, where a reduced window of data being recorded (instead of typical values of 10 to 120 s of data) can be used to detect BRB_{sbf}, and an estimation of current signal parameters could be obtained, hence with the estimated parameters of the current waveform, the detection of BRB_{sbf} could be more accurate. Prony method literature defines the parameters of a signal model $y(t)$ in (2), and they can be obtained by sampling the signal and obtaining the data samples $[y(1)\ y(2)\ \ldots\ y(n)]$ using a sampling frequency f_s.

$$y(t) = \sum_{n=1}^{N} A_n e^{\sigma_n t} \cos(2\pi f_n t + \theta_n) \tag{2}$$

The Prony model signal approximates the sampled data in (2) using the following linear combination of p complex exponentials:

$$y_M = \sum_{n=1}^{p} B_n \lambda_n^M \tag{3}$$

$$B_n = \frac{A_n}{2} e^{j\theta_n}$$

$$\lambda_n = e^{(\sigma_n + j2\pi f_n)T}$$

The signal $y(t)$ in (2) has four elements: magnitude A_n, damping factor σ_n, frequency f_n, and the phase angle θ_n. Each exponential term in (3) is a unique signal mode of the original signal $y(t)$. So, using the Euler theorem and total time $t = MT$, where M is the length of the signal and T is the time between samples, Equation (2) can be rewritten as (3).

So, for the Prony method to be implemented in OTD for RCIM, the following steps should be considered:

(1) Know the sampling frequency (f_s), sampling time (T_s), length of the current signal under analysis (L) with a minimum of 25 cycles of data and the order (p) of the linear prediction model (LPM), where an initial value of p for a data window of current signal measurement for analysis must be selected.

(2) A Toeplitz matrix "$\boldsymbol{Y}$" with the data of the current signal "$y(t)$" must be defined as (4).

$$\boldsymbol{Y} = \begin{bmatrix} y[p] & y[p-1] & \cdots & y[1] \\ y[p+1] & y[p] & \cdots & y[2] \\ \vdots & \vdots & \ddots & \vdots \\ y[2p-1] & y[2p-2] & \cdots & y[p] \end{bmatrix} \tag{4}$$

(3) A vector "$\boldsymbol{a}$" (coefficients of characteristic Equation (3)) using (4) is calculated in (5).

$$\begin{bmatrix} a[1] \\ a[2] \\ \vdots \\ a[p] \end{bmatrix} = \begin{bmatrix} y[p] & y[p-1] & \cdots & y[1] \\ y[p+1] & y[p] & \cdots & y[2] \\ \vdots & \vdots & \ddots & \vdots \\ y[2p-1] & y[2p-2] & \cdots & y[p] \end{bmatrix}^{-1} \cdot \left(- \begin{bmatrix} y[p+1] \\ y[p+2] \\ \vdots \\ y[2p] \end{bmatrix} \right) \tag{5}$$

(4) Calculate the roots from vector "$\boldsymbol{a}$" and the resulting roots vector "$\boldsymbol{z}$" will be used in (6) and (7) to calculate damping

$$\sigma = \frac{ln|\boldsymbol{z}|}{T_s} \tag{6}$$

and frequency

$$f = \frac{1}{2\pi T_s} tan^{-1}\left(\frac{Im(\boldsymbol{z})}{Re(\boldsymbol{z})}\right) \tag{7}$$

(5) Obtain Vandermonde matrix "$\boldsymbol{Z}$" of vector "$\boldsymbol{z}$" using (8).

$$\boldsymbol{Z} = \begin{bmatrix} z_1^0 & z_2^0 & \cdots & z_p^0 \\ z_1^1 & z_2^1 & \cdots & z_p^1 \\ \vdots & \vdots & \ddots & \vdots \\ z_1^{p-1} & z_2^{p-1} & \cdots & z_p^{p-1} \end{bmatrix} \tag{8}$$

(6) Obtain vector "$\boldsymbol{h}$" in (9) using vandermonde matrix "$\boldsymbol{Z}$" and vector "$\boldsymbol{y}$" from (8).

$$\begin{bmatrix} h_1 \\ h_2 \\ \vdots \\ h_p \end{bmatrix} = \begin{bmatrix} z_1^0 & z_2^0 & \cdots & z_p^0 \\ z_1^1 & z_2^1 & \cdots & z_p^1 \\ \vdots & \vdots & \ddots & \vdots \\ z_1^{p-1} & z_2^{p-1} & \cdots & z_p^{p-1} \end{bmatrix}^{-1} \cdot \begin{bmatrix} y[1] \\ y[2] \\ \vdots \\ y[p] \end{bmatrix} \tag{9}$$

(7) The resulting vector "$\boldsymbol{h}$" obtained in (9) will be used in (10) and (11) to calculate amplitude and phase angle.

$$A = |\boldsymbol{h}| \tag{10}$$

$$\theta = tan^{-1}\left(\frac{Im(\boldsymbol{h})}{Re(\boldsymbol{h})}\right) \tag{11}$$

(8) The order for good estimation results is obtained evaluating the mean square error (MSE) of the full signal data p = 1, 2, … , N_s, where N_s is the total data samples of the selected data signal for analysis. The MSE for each value of p in (12) needs to be calculated, where MSE is obtained by using the reconstructed signal with the estimated parameters "$\hat{y}_j$" and the real signal "y_j", so the MSE of lesser magnitude is selected for the corresponding p value is the optimum estimate of the model signal parameters.

$$MSE_p = x_p = \frac{1}{N_s}\sum_{j=1}^{N_s}\left(\hat{y}_j - y_j\right)^2 \tag{12}$$

Some important considerations in Prony estimation has to be taken to implement this parametric estimation method in OTD for BRB_{sbf} detection: (1) The sampled current signal must be analyzed, (2) the sampling rate must be known; (3) if noise in the signal or other harmonics of no interest exist, the signal must be filtered; (4) an increase in computational burden will occur if a higher number of samples of digitized current signals are considered. It should be mentioned that the accuracy of Prony estimation depends on the level of signal distortion, the observation data window, and the number of samples used in the estimation process, as well as the order of the model [11]. Prony method is a good alternative for increasing the sensitivity and accuracy of the OTD for RCIM diagnostics for BRB_{sbf} detection.

4. Study Case for Motor Current Signal Analysis Using Prony Method Estimation

In this section, an assessment of Prony method estimation using a simulated and real current signal with BRB harmonic components is presented. The simulated current signal for analysis includes two BRB_{sbf}, and for the real current signal analysis, a laboratory test system with a data acquisition system, a RCIM with broken rotor bars and VFD are used,

where the motor current signals are recorded at full load condition at nominal speed (60 Hz) and at different operating speeds. This will allow to perform a complete evaluation and validation of the method for OTD of RCIM diagnostics application.

4.1. Assessment of Numerical Simulation of Broken Rotor Bar Current Signal

For this analysis, the simulated current signal considering two side band frequencies is used to estimate its signal parameters using Prony method, as presented in (6), (7), (10), and (11). In Figure 3, 2 s simulated signal is used for the analysis, where the full signal considers two sideband frequencies and its individual frequency components are shown for a fundamental frequency of 60 Hz and a slip value of 0.0089 describing the behavior of a loaded motor, where (1) is used to obtain the two sideband frequencies in the signal, so the signal in Figure 3a can be used for the Prony analysis. In Table 2, the harmonic order, frequency, amplitude of fundamental frequency, and the calculated BRB_{sbf} of the signal in Figure 3 that will be used for the analysis are presented.

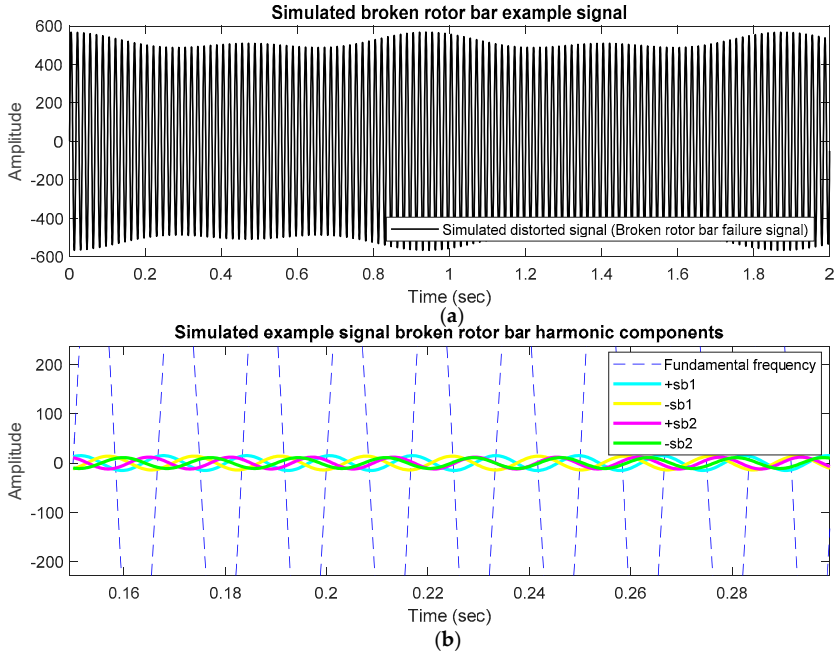

Figure 3. Simulated signal example. (**a**) Distorted signal. (**b**) Broken rotor bar harmonic components.

Table 2. Simulated example signal with broken rotor bar harmonic components.

Harmonic Order	Frequency, (Hz)	Amplitude
1	60	516
1.0178	61.06 (+sb1)	15
0.9822	58.93 (−sb1)	14
1.0356	62.13 (+sb2)	12
0.9644	57.86 (−sb2)	11

Prony Estimation Results

The signal in Figure 3a is used for analysis with a sampling frequency of 64 samples per cycle and a window of data of 8 cycles. The sampling frequency of 64 samples/cycle and 8 cycles of window data length are considered because with a fixed data window with lesser data a good and accurate estimation could be achieved. It is important to mention that with more data considered for the estimation process (more than 8 cycles for simulated signal in Figure 3a), an increase in computational burden will occur and more time will

be required to obtain accurate estimated frequencies and amplitudes. In Figure 4a, the Prony estimated and original signal are compared, and it can be observed that there is no considerable error between them, and the estimated spectrum in Figure 4b of signal in Figure 4a is obtained from the Prony estimation results calculated from (7) and (10), the estimation results are presented in Table 3.

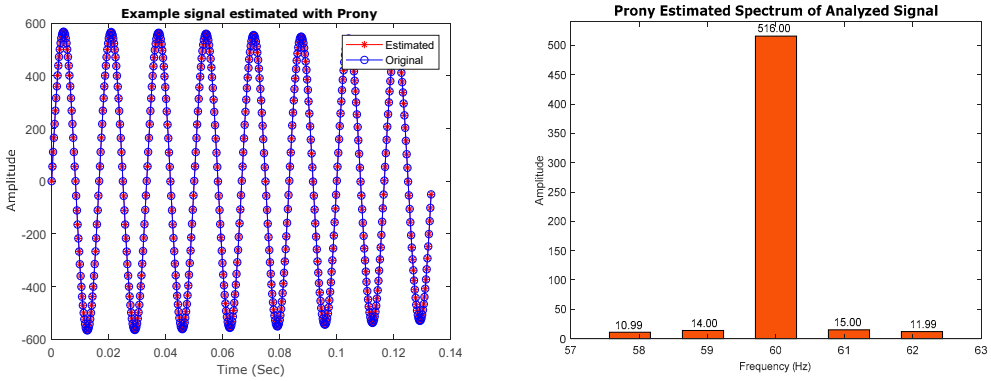

Figure 4. Simulated example signal validation. (**a**) Estimated and original signal comparison. (**b**) Estimated Prony spectrum.

Table 3. Simulated example, Prony estimated signal parameters.

Estimated Signal Parameters	Frequency, (Hz)	Amplitude
Example signal	60	516.00
	61.06	15.00
	58.93	14.00
	62.13	11.99
	57.86	10.99

The Prony estimation results in Table 3 are obtained using a defined window of data of the simulated example signal in Figure 3a; 8 cycles and a sampling frequency of 64 samples per cycle are considered. Only the estimated signal amplitude and frequency are presented in Table 3, because these parameters are the ones that can be used to detect BRB_{sbf} of the signal under analysis. It should be mentioned that the damping results and phase angle of the signal parameter estimation correspond to the model of the Prony signal presented in Equation (2) and are required only to form the estimated Prony signal and then the MSE is calculated so the optimum parameter estimates could be obtained. Good estimation results can be achieved considering a window data length of 8 cycles and a sampling frequency of 64 samples per cycle for the detection of two sideband frequencies for broken rotor bars.

4.2. Assessment of Real Broken Rotor Bar Current Signal from a Laboratory Test System

For this analysis, a laboratory test system considering a $\frac{1}{2}$ HP RCIM with a crack in one ring of the rotor, a data acquisition system, and a VFD are used for the current signal analysis using the Prony method; it should be mentioned that different operation conditions are considered for the analysis. Moreover, a comparison of FFT results and Prony estimation results are presented so that the advantages of using Prony method can be highlighted for OTD application.

4.2.1. Laboratory Test System

In Figure 5, the laboratory test system used for the data acquisition of current signals of the RCIM under analysis is presented. For the analysis, the current signals are required, so the signals are measured at the motor terminals; in Figure 5a, a VFD is used to control

the speed of the RCIM which will be operating at full load condition. The nameplate data of the RCIM are as follows 208 V, 1.98 A, 60 Hz, 1730 rpm and are presented in Appendix A in Table A1. In Figure 5b, the load is set at 2.05 N-m, which is the condition for full load operation for the RCIM. In Figure 5c, the data acquisition system used is a National Instruments cRIO-9045 with LabVIEW software and Tektronix current sensors A622 with the setting of 100 mv/A. Figure 6 shows the RCIM rotor of RCIM in Figure 5b which has a cracked ring and a broken rotor bar.

Figure 5. Laboratory test system. (**a**) Full system. (**b**) RCIM under analysis and its load. (**c**) National Instruments data acquisition system compact RIO.

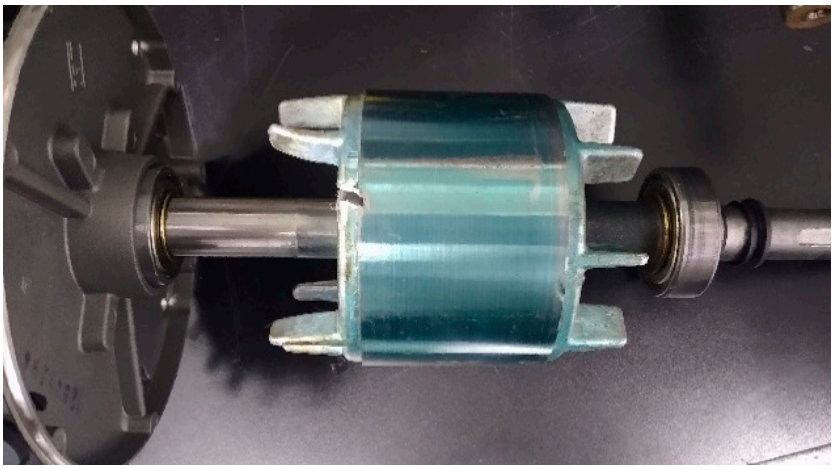

Figure 6. RCIM cracked ring rotor and broken rotor bar for analysis.

Figure 7 presents the current signal measurement of motor line current of phase A, only 1 s of the recorded signal of the 5 s total length is presented for visualization purposes, current signal in Figure 7 was obtained at 60 Hz operation of the motor (full speed), and full load condition without the operation of the VFD. It should be mentioned that the sideband frequencies considered for the detection of the cracked ring or broken rotor bar were calculated with (1) considering a full load slip of 0.0388, 2 sideband frequency components were calculated for 60 Hz as fundamental component: 64.66 Hz, 55.33 Hz, 69.33 Hz, and 50.66 Hz. Hence, the signal in Figure 7 will be used for the Prony analysis and FFT analysis for 60 Hz. In the following sections, current signal measurements at different VFD speed operation conditions (50 Hz, 40 Hz, 30 Hz, 20 Hz, and 10 Hz) are analyzed to validate the

proposed Prony method for OTD application in RCIM, and FFT will also be analyzed to compare and highlight the advantages of using Prony method for OTD in RCIM.

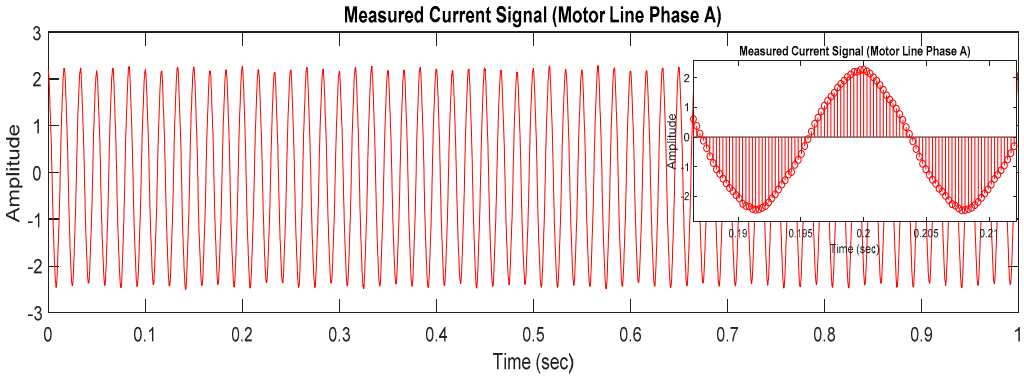

Figure 7. Current signal measurement of motor line current of phase A with a sampling frequency of 64 samples per cycle at 60 Hz with no VFD operation.

4.2.2. Fast Fourier Transform Estimation Results

In this section a FFT analysis of the measured current signals from the test system in Figure 5 is performed using the VFD. For the purpose of analysis, only motor line current of Phase A is considered and the length of the recorded signal is 5 s. The sampling frequency of the signal is 64 samples per cycle, and the FFT estimation results are presented for different speed operations at full load of the RCIM; the output frequencies for the VFD, which are related to rotor speeds, are 60 Hz, 50 Hz, 40 Hz, 30 Hz, 20 Hz, and 10 Hz.

It could be observed that for a signal record of 5 s, for every speed variation 60 Hz, 50 Hz, 40 Hz, 30 Hz, 20 Hz, and 10 Hz in Figures 8–13, the sideband frequencies considered for each speed operation condition are not detected. It should be mentioned that at least 10 s of the signal must be recorded to determine if a problem with the rotor is present, as described in Section 2. Table 4 presents two sideband frequencies of the RCIM calculated from (1) for each speed operation condition frequency. BRB_{sbf} will be used to compare the results obtained from the FFT estimations and also the information defined in Table 1.

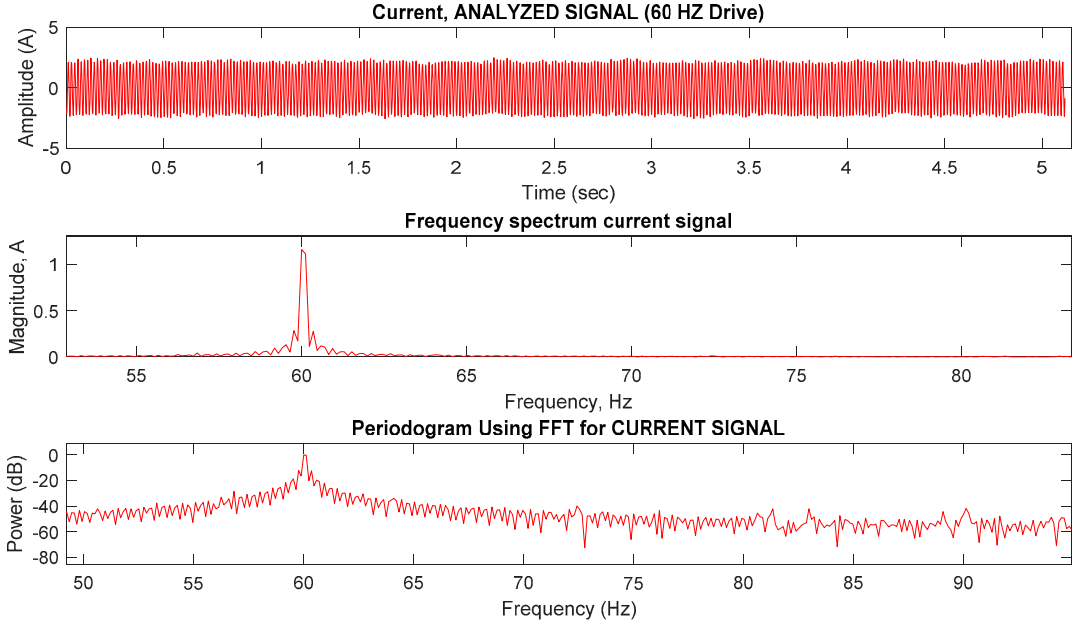

Figure 8. FFT analysis of current signal measurement of motor line current of phase A, frequency spectrum, and periodogram at 60 Hz speed operation.

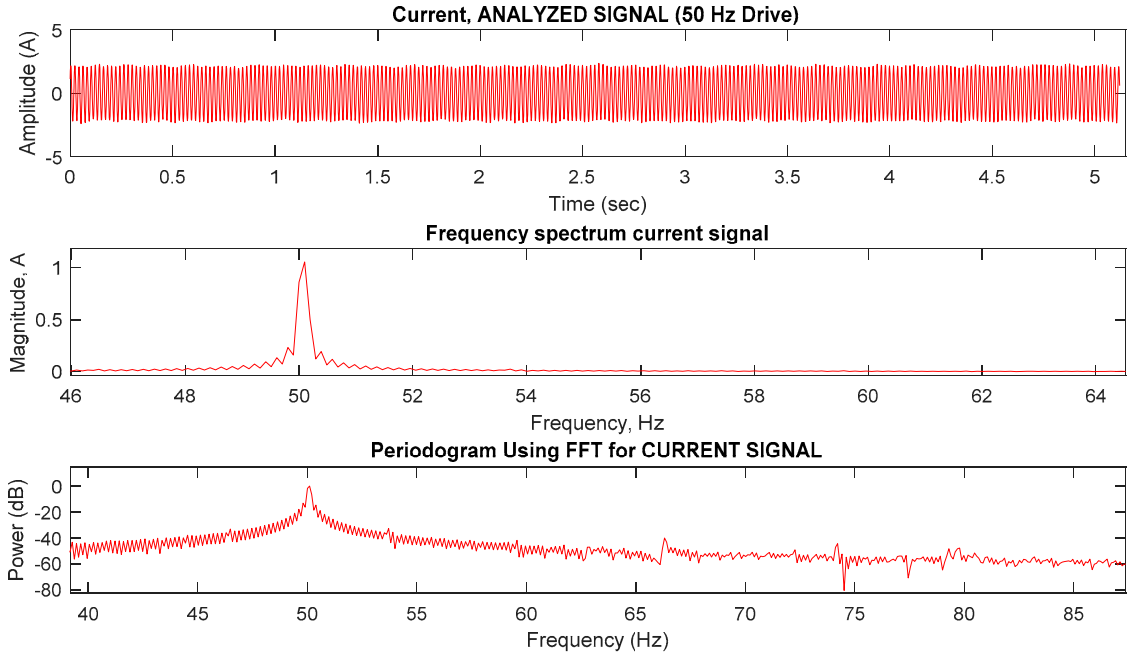

Figure 9. FFT analysis of current signal measurement of motor line current of phase A, frequency spectrum, and periodogram at 50 Hz speed operation.

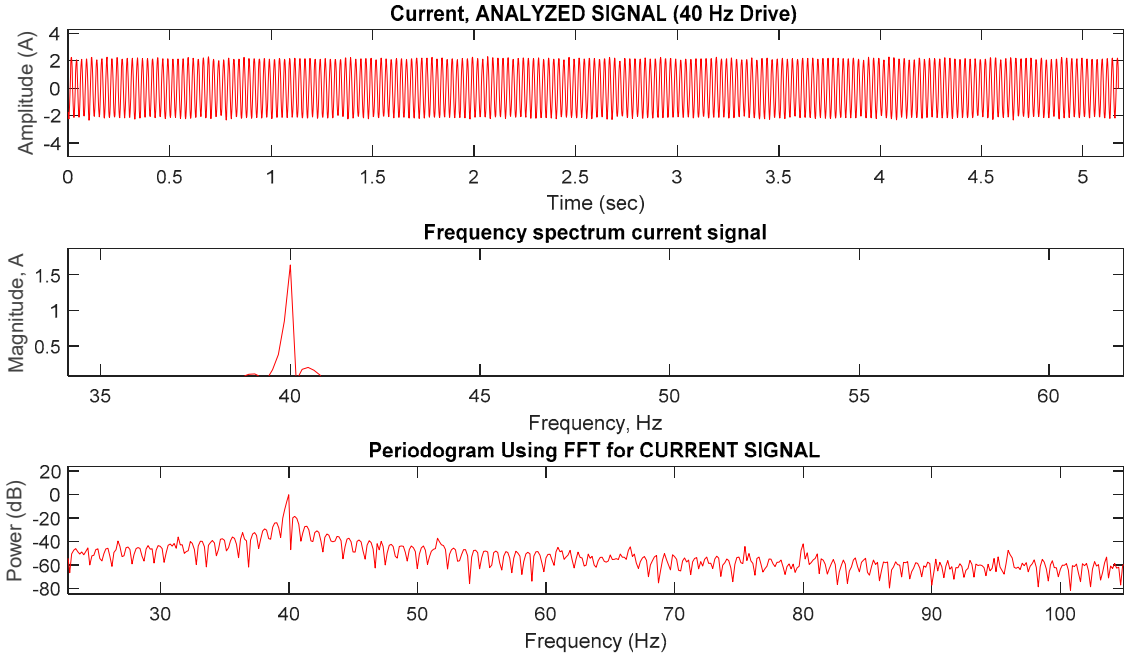

Figure 10. FFT analysis of current signal measurement of motor line current of phase A, frequency spectrum, and periodogram at 40 Hz speed operation.

As shown in FFT spectrum and periodogram from Figures 8–13 and Table 5, frequencies presented in Table 4 are not detected for each VFD speed operation condition, only the fundamental frequency is detected. This occurs mainly due to the closeness of the frequencies to the fundamental frequency, where more signal data are required (at least 10 s) so the FFT could detect the sideband frequencies. The periodogram is included because it is used to highlight the sideband frequencies in dB, which is the unit where a severity of a faulted rotor of RCIM can be measured, as it is presented in Table 1. Hence, one of the disadvantages of the FFT analysis for OTD for RCIM, is that it is not possible for the

detection of the BRB_{sbf} with less than 10 s of recorded current signal, where it is evident in the results from Figures 8–13 and Table 5 that the sideband frequencies are not detected, so larger data windows and no variations in load of the motor under analysis are required for FFT analysis to detect BRB_{sbf}.

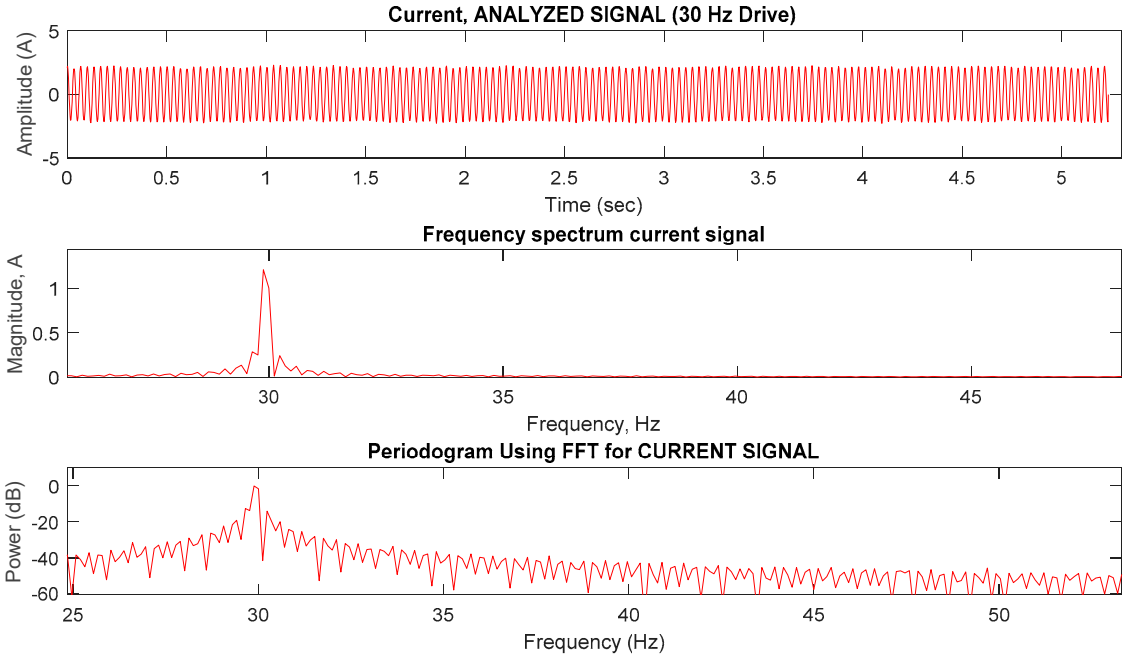

Figure 11. FFT analysis of current signal measurement of motor line current of phase A, frequency spectrum, and periodogram at 30 Hz speed operation.

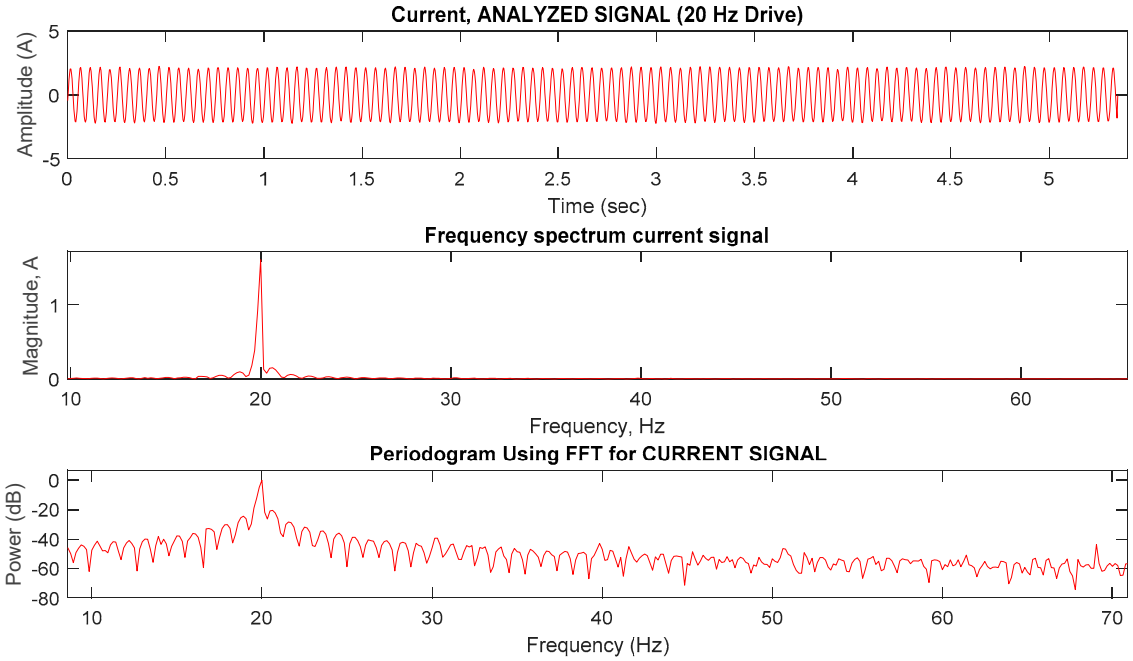

Figure 12. FFT analysis of current signal measurement of motor line current of phase A, frequency spectrum, and periodogram at 20 Hz speed operation.

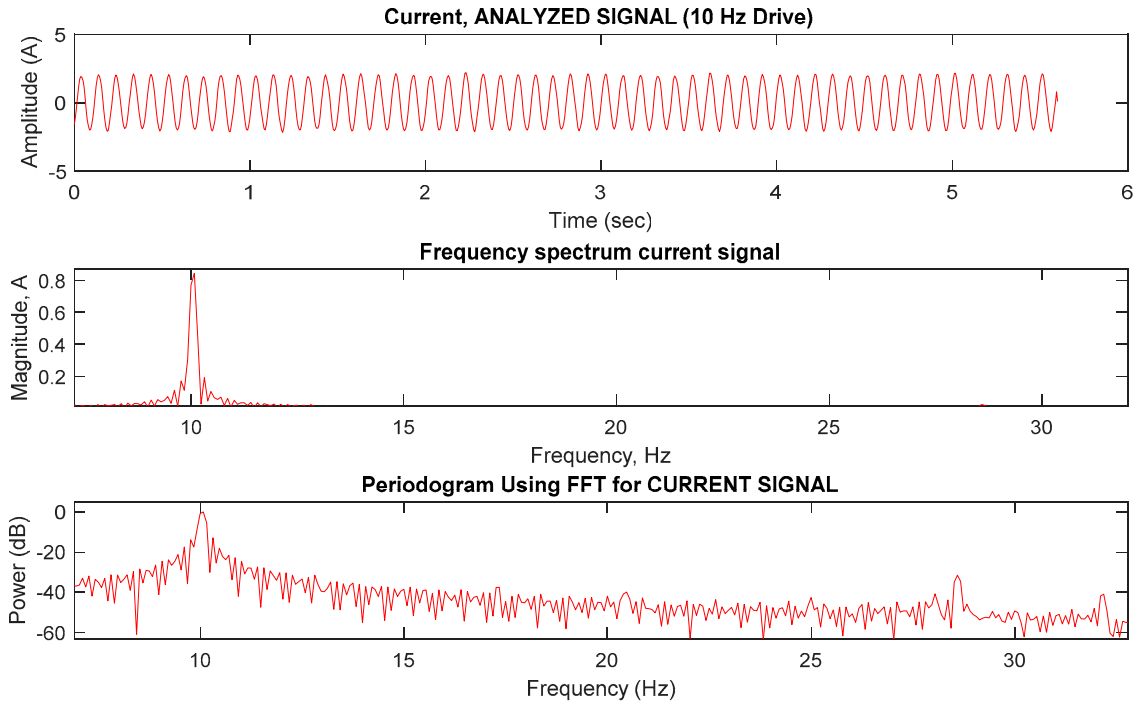

Figure 13. FFT analysis of current signal measurement of motor line current of phase A, frequency spectrum, and periodogram at 10 Hz speed operation.

Table 4. BRB_{sbf} for each speed operation condition at VFD.

Full Load Slip, (s)	Sideband Frequencies	Frequency, (Hz)					
0.0388	Speed operation Condition, Fundamental frequency	60	50	40	30	20	10
	Sb1+	64.66	53.88	43.11	32.33	21.55	10.77
	Sb1−	55.33	46.11	36.88	27.66	18.44	9.22
	Sb2+	69.33	57.77	46.22	34.66	23.11	11.55
	Sb2−	50.66	42.22	33.77	25.33	16.88	8.44

4.2.3. Prony Estimation Results

In this section, the proposed Prony method estimation for OTD application for RCIM diagnostics is evaluated for different speed operation conditions of a RCIM at full load using the test system in Figure 5. The recorded signals used for the analysis are the current signals from Figures 8–13 for each speed operation condition, where the difference between the analysis from FFT and Prony, is that the estimation of signal frequency and amplitude parameters will be obtained only by considering 25 cycles of each signal instead of 5 s. The sampling frequency of the signals is the same for each one of the 64 samples per cycle. The following steps should be followed to obtain the optimum signal parameters of frequency and amplitude, so we can search the BRB_{sbf} presented in Table 4 in the Prony estimation results. First, a downsampling of the signal under analysis is required. Then, the downsampled signal needs to be filtered (low pass filter and a DC filter), so that Prony can estimate the frequencies with a minimum error, because the method is sensitive to noise. Next, the downsampled and filtered signal is used for the Prony estimation calculation as presented in Section 3.

Table 5. FFT results for each speed operation condition at VFD.

Estimated Signal Parameters	True Frequency Values (Hz)		FFT Estimation Results		
			Frequency (Hz)	Amplitude (A)	Power (dB)
Full Load Slip s = 0.0388	(1 + 2 s) f [Sb1−]	55.33	59.77	0.285	−12.20
	Fundamental (f)	60.00	60.00	1.161	0
	(1 − 2 s) f [Sb1+]	64.66	60.35	0.277	−12.42
	(1 + 2 s) f [Sb1−]	46.11	49.8	0.232	−13.16
	Fundamental (f)	50.00	50.1	1.055	0
	(1 − 2 s) f [Sb1+]	53.88	50.39	0.192	−14.76
	(1 + 2 s) f [Sb1−]	36.88	39.06	0.104	−23.9
	Fundamental (f)	40.00	40.00	1.641	0
	(1 − 2 s) f [Sb1+]	43.11	40.47	0.196	−18.44
	(1 + 2 s) f [Sb1−]	27.66	29.65	0.285	−12.58
	Fundamental (f)	30.00	29.88	1.216	0
	(1 − 2 s) f [Sb1+]	32.33	30.23	0.241	−14.03
	(1 + 2 s) f [Sb1−]	18.44	18.91	0.096	−24.41
	Fundamental (f)	20.00	20.00	1.61	0
	(1 − 2 s) f [Sb1+]	21.55	20.63	0.151	−20.52
	(1 + 2 s) f [Sb1−]	9.22	9.21	0.108	−23.1
	Fundamental (f)	10.00	10.00	1.543	0
	(1 − 2 s) f [Sb1+]	10.77	11.41	0.071	−26.68

Downsampling

The recorded current signal is considered at 64 samples per cycle; nevertheless, a downsampling to 16 samples per cycle, as shown in Figure 14, is recommended to reduce the computational effort during the estimation process with Prony method (if a real time application is considered), and it is justified that due to the low frequencies (BRB_{sbf}) that are required to estimate there is no need for a high resolution recorded signal. This condition could be modified according to the needs of specific frequency detection for diagnostics application in MCSA.

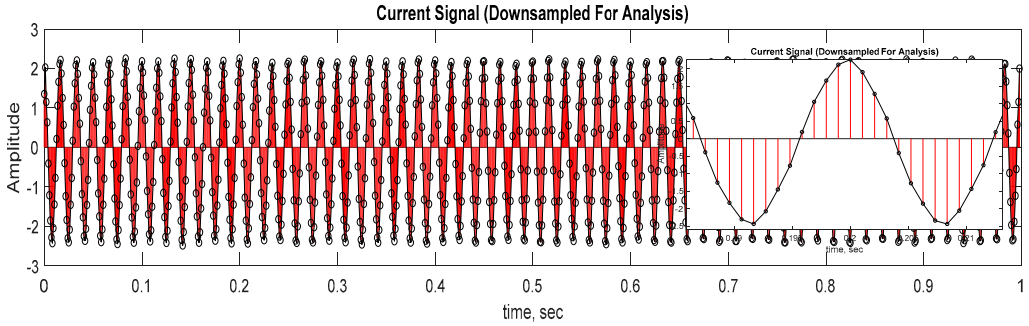

Figure 14. Downsampled current signal of measurement of motor line current of phase A at 60 Hz operation.

Low Pass and DC Filter

As mentioned in Section 3, if the recorded signal under analysis includes noise or other harmonics of no interest, the signal must be filtered to eliminate unwanted frequencies, so that the Prony estimation could be accurate. This step is carried out prior to using the signal

as input signal for the estimation of signal parameters. For this particular application, a low pass filter of order 4 with a cut off frequency of harmonic order of 5 (300 Hz for 60 Hz) is used, see Figure 15; it is important to consider that the cutoff frequency will change if a VFD with a specific speed frequency operation (change in fundamental frequency) is considered. Moreover, a DC filter should be considered after the low pass filter, mainly because in a recorded signal, a DC offset will appear due to the measurement equipment (current sensors), see Figure 16, some equipment have zero adjustment to prevent a DC offset to appear in a recorded signal. If low pass filter and DC filter are not considered in signal processing prior to using the signal for Prony estimation it can cause a significant error in the estimated signal parameters, or other non-real frequencies will appear in the estimation results which can lead to a misinterpretation or a misdiagnosis.

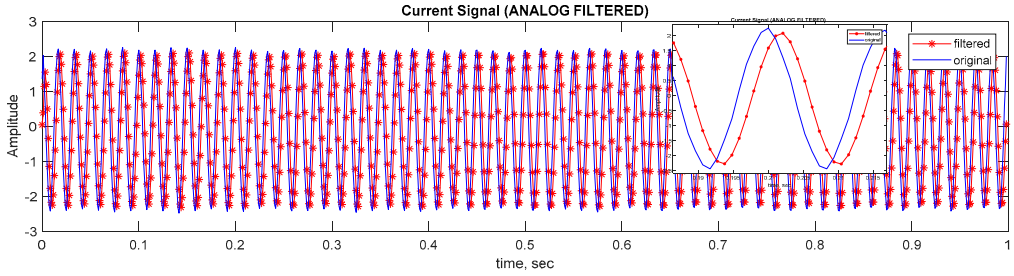

Figure 15. Downsampled low pass filtered current signal of measurement of motor line current of phase A at 60 Hz operation.

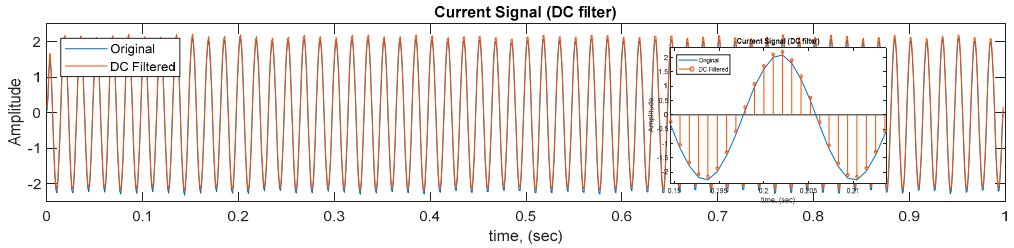

Figure 16. Downsampled low pass filtered and DC filtered current signal of measurement of motor line current of phase A at 60 Hz operation.

Signal Parameter Estimation

In order to obtain a good estimate of signal parameters using Prony method for OTD in RCIM, the considerations mentioned in Section 3 and Sections Downsampling and Low Pass and DC Filter must be applied, then the current signal under analysis, see Figure 17, will be used as the input signal to obtain the parameter estimation. It should be mentioned that a sliding window of data is used in this section to obtain the estimates, in the first analysis are considered only 5 sliding data windows for 60 Hz operation speed, where at each window of data a set of estimated parameters will be obtained with the main purpose to validate Prony method estimation application to detect BRB_{sbf}. Then, an analysis of one data window for each speed frequency operation with VFD (50 Hz, 40 Hz, 30 Hz, 20 Hz, and 10 Hz) is considered, and the BRB_{sbf} to be detected will be the ones indicated in Table 4. Hence, it is important to mention that the window length of data to be analyzed will be of 25 cycles for each speed operation condition.

Once the input signal to the Prony method has been digitally processed under the considerations mentioned in Sections Down Sampling and Low Pass and DC Filter, it now can be used in Prony method to determine an accurate estimate of signal parameters and BRB_{sbf}. Table 6 shows the estimation results using the methodology described in Section 3, where in order to validate the Prony estimation results five sliding data window are considered, so five calculations of Prony method are made, so the reader can observe that the estimated frequencies and its amplitudes correspond to the BRB_{sbf} defined in Table 4; also, it could be observed that a third pair of sideband frequencies also is detected.

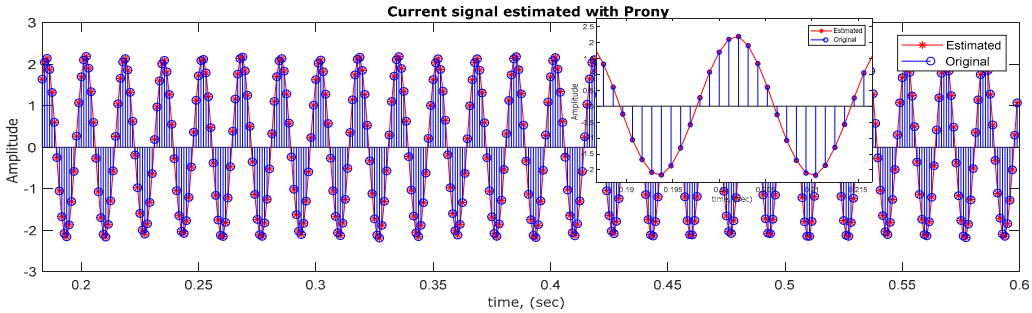

Figure 17. Sliding data window (Prony estimated and original signal) of 25 cycles of current signal measurement of motor line current of phase A at 60 Hz operation.

Table 6. Measured current signal estimated parameters.

Estimated Signal Parameters	Data Window 1		Data Window 2		Data Window 3		Data Window 4		Data Window 5	
	Frequency (Hz)	Amplitude	Frequency (Hz)	Amplitude	Frequency (Hz)	Amplitude	Frequency (Hz)	Amplitude	Frequency (Hz)	Amplitude
Sb3—	44.03	0.0536	44.03	0.0540	43.97	0.0551	43.90	0.0566	43.91	0.0552
Sb2—	51.28	0.0207	51.28	0.0208	51.30	0.0206	51.26	0.0149	51.25	0.0162
Sb1—	55.44	0.0426	55.44	0.0427	55.46	0.0423	55.42	0.0385	55.44	0.0391
Fundamental	60.02	2.1440	60.02	2.1441	60.02	2.1444	60.02	2.1418	60.02	2.1425
Sb1+	64.71	0.0279	64.71	0.0278	64.69	0.0273	64.68	0.0291	64.66	0.0284
Sb2+	69.66	0.0197	69.68	0.0195	69.72	0.0182	69.55	0.0204	69.58	0.0182
Sb3+	75.96	0.0248	75.97	0.0248	75.97	0.0248	75.97	0.0251	75.98	0.0250

To determine the severity condition of the rotor, the energy in dB needs to be obtained from a periodogram spectrum and to be compared with rotor fault signature in Table 1. First, the frequency spectrum of the results obtained for each sliding data window in Table 6 is presented in Figure 18, then, with the information obtained in Table 6, energy is plotted in a periodogram as shown in Figure 19. It could be observed that with frequency spectrum low magnitudes are observed, this is the main reason of the periodogram importance to plot these magnitudes in energy values in dB, so the BRB_{sbf} of the RCIM under analysis could be more evident.

As observed in Figure 19, the energy levels are between 31.56 and 41.42 dB of the BRB_{sbf} for the sliding data windows evaluated, the energy estimated values correspond to multiple cracked or broken bars or in its case a ring problem as described in Table 1. In Figure 6, a cracked ring rotor and broken rotor bar is used in the test system to perform the current signal analysis, so it is evident that an accurate diagnostic could be achieved with Prony method parameter estimation.

To complete the most common operative scenarios of RCIM for the experimental validation of Prony method, as described in Section 4.2, current signals are measured at motor line terminal phase A in the laboratory test system from Figure 5 using a VFD at different speed operation conditions defined in Table 4, at full load condition, where also its BRB_{sbf} are determined so a diagnostic of the RCIM can be obtained from the Prony estimation results.

In Figure 20, the digitally processed current signals (original) for each frequency speed operation are compared with the Prony estimated signal obtained from (2) using the estimated parameter results in Table 7, it can be observed in Figure 20 that for each VFD operation frequency the difference between the signals is null, this can be quantified by calculating MSE curve fitting in (12), the MSE curve fitting results has a value of 1.7889×10^{-4} for 50 Hz, 5.2202×10^{-4} for 40 Hz, 6.4835×10^{-4} for 30 Hz, 4.6944×10^{-4} for 20 Hz, and 2.4833×10^{-4} for 10 Hz; these results confirm that an accurate estimate of the BRB_{sbf} and diagnostic is achieved.

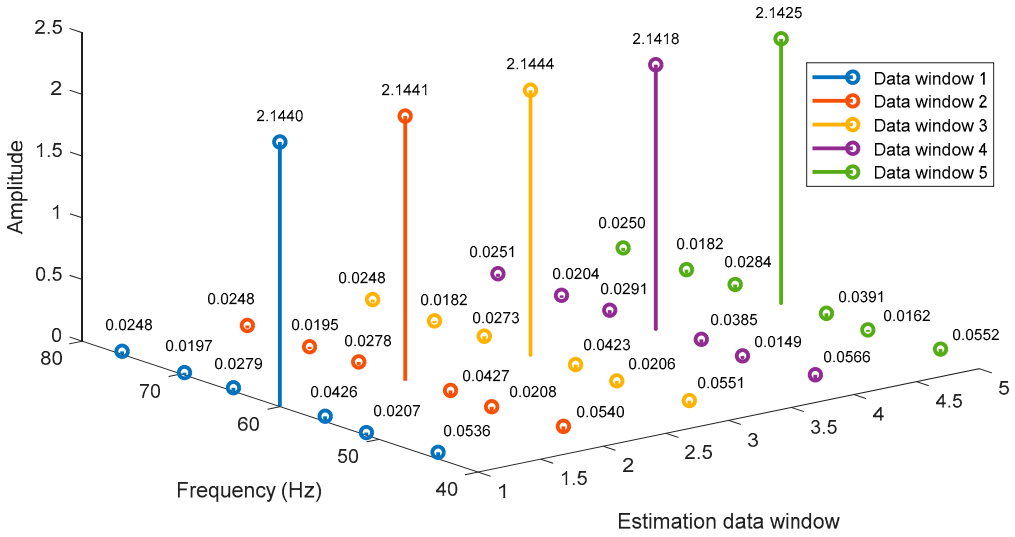

Figure 18. Prony estimated frequency spectrum at 60 Hz frequency speed operation scenario.

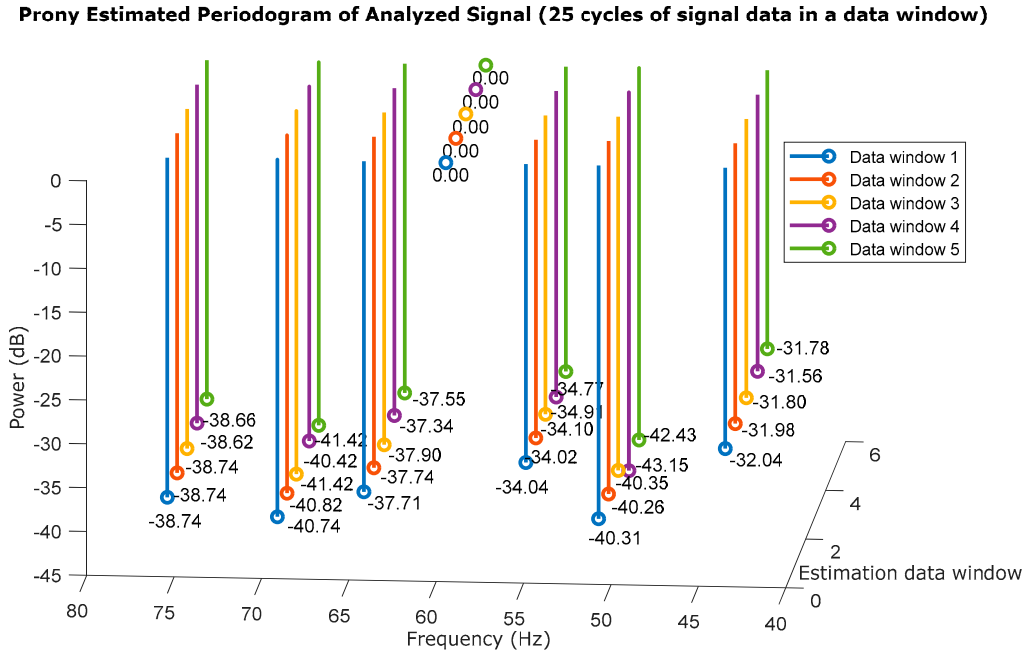

Figure 19. Prony estimated periodogram at 60 Hz frequency speed operation scenario.

In Table 7, the Prony estimation results of signal parameters are presented, where it can be observed that for each VFD speed operation, its sideband frequencies (True frequency values), amplitudes, and energy in dB are accurately estimated, where the obtained energy in dB corresponds to the real damage severity condition presented in Table 1 of the rotor of the RCIM under analysis. First, the frequency spectrum of the results obtained for each VFD speed operation frequency in Table 7 is presented in Figure 21, then, for visualization purpose of the results 7, the Periodogram for each Prony estimated signal parameters from Figure 20 is presented in Figure 22, where its fundamental frequency is normalized to 0 dB.

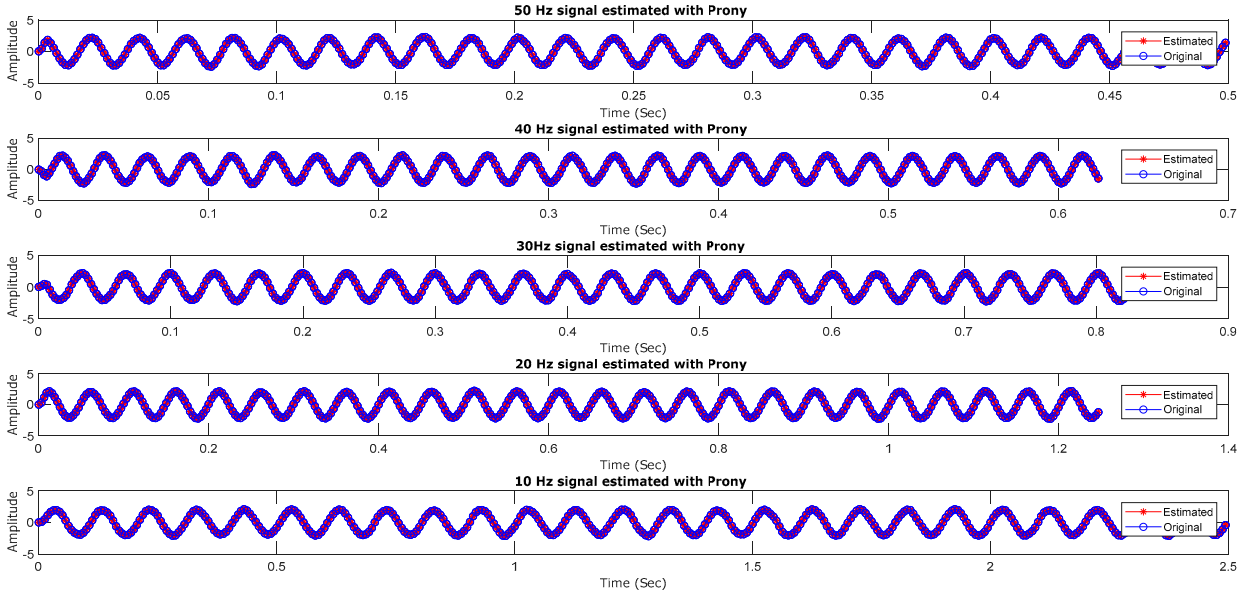

Figure 20. Data window selected for analysis of 25 cycles of current signal measurement of motor line current of phase A at VFD operation frequencies of 50 Hz, 40 Hz, 30 Hz, 20 Hz, and 10 Hz (Prony estimated and original signal).

Table 7. Measured current signal estimated parameters (VFD, motor at full load).

Estimated Signal Parameters	Measured Signal (Current Phase A)					
	True Frequency Values (Hz)		Prony Method Estimation Results			
			Frequency (Hz)	Amplitude (A)	Power (dB)	MSE Curve Fitting
Full Load Slip s = 0.0388	(1 + 2 s) f [Sb1−]	46.11	46.89	0.0222	−39.76	1.7889×10^{-4}
	Fundamental (f)	50.00	50.07	2.1599	0	
	(1 − 2 s) f [Sb1+]	53.88	54.16	0.0192	−41.02	
	(1 + 2 s) f [Sb1−]	36.88	36.50	0.0327	−36.41	5.2202×10^{-4}
	Fundamental (f)	40.00	39.96	2.1628	0	
	(1 − 2 s) f [Sb1+]	43.11	43.64	0.0140	−43.78	
	(1 + 2 s) f [Sb1−]	27.66	26.78	0.0231	−39.37	6.4835×10^{-4}
	Fundamental (f)	30.00	29.92	2.1475	0	
	(1 − 2 s) f [Sb1+]	32.33	33.23	0.0424	−34.09	
	(1 + 2 s) f [Sb1−]	18.44	18.01	0.0400	−34.41	4.6944×10^{-4}
	Fundamental (f)	20.00	19.95	2.1011	0	
	(1 − 2 s) f [Sb1+]	21.55	21.59	0.0277	−37.60	
	(1 + 2 s) f [Sb1−]	9.22	9.68	0.0305	−36.39	2.4833×10^{-4}
	Fundamental (f)	10.00	10.05	2.0117	0	
	(1 − 2 s) f [Sb1+]	10.77	10.60	0.0420	−33.61	

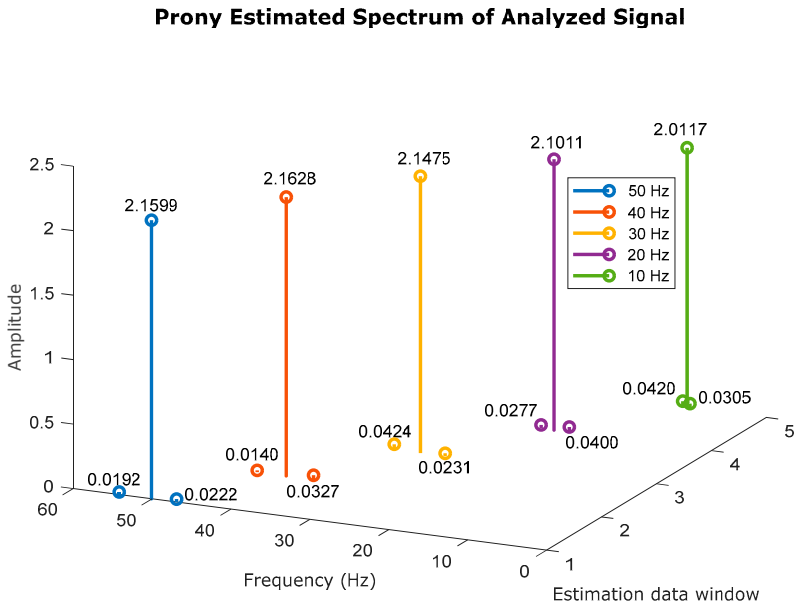

Figure 21. Prony estimated spectrum of VFD frequency speed operation scenarios.

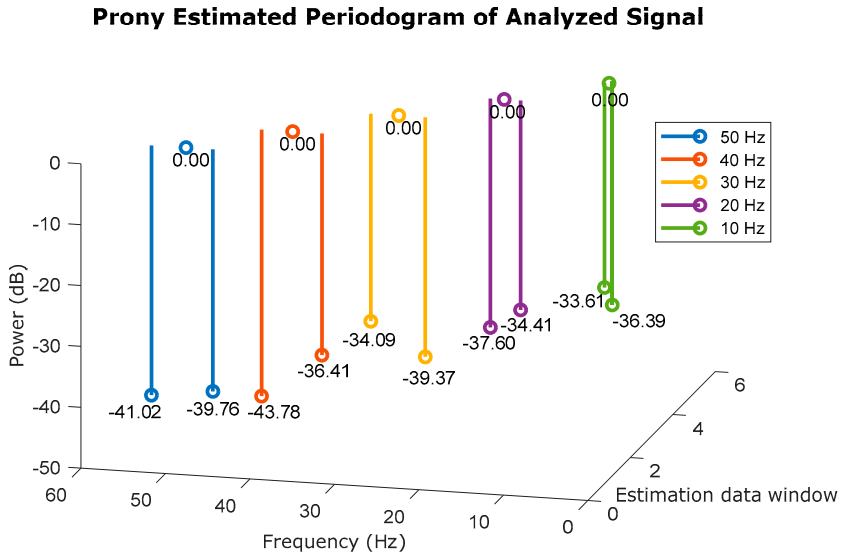

Figure 22. Prony estimated periodogram of VFD frequency speed operation scenarios.

5. Results and Discussion

A results comparison is performed between FFT analysis (using a 5 s recorded current signal) and Prony method (using a 25 cycles of recorded current signal) in this work. It is important to mention that 25 cycles have been selected because that is the minimum data window length with good and accurate results, other tests from 1–24 cycles were performed but no good estimation is achieved, so the best possible application option for online test diagnostics equipment with the minimum possible estimation time is 25 cycles. Moreover, a very important detail to mention is that the computational estimation time increase exponentially for each increase in the sampling frequency, so this is the main reason why a subsampling to 16 samples per cycle is considered. In Sections 4.2.2 and 4.2.3, the estimation results at different VFD speed operation conditions are presented, and Table 8 shows a summary of the results for both methods. Note from Table 8 that for each VFD speed operation condition, the FFT results are not accurate and BRB_{sbf} cannot be detected having a 5 s recorded signal, but if Prony estimation results are observed and compared with the True frequency values, then use Table 1 to determine the severity condition of

the cage of the rotor, it can be validated that the estimated energy in dB corresponds to a cracked ring and/or BRB, which is the real condition of the rotor shown in Figure 6.

Table 8. Summary of current signal estimated parameters using FFT and Prony method (VFD, motor at full load).

Estimated Signal Parameters	Measured Signal (Current Phase A)								
	True Frequency Values (Hz)		FFT Estimation Results			Prony Method Estimation Results			
			Frequency (Hz)	Amplitude (A)	Power (dB)	Frequency (Hz)	Amplitude (A)	Power (dB)	MSE Curve Fitting
Full Load Slip s = 0.0388	(1 + 2 s) f [Sb1−]	55.33	59.77	0.285	−12.20	55.44	0.0426	−34.04	6.4593×10^{-4}
	Fundamental (f)	60.00	60.00	1.161	0	60.02	2.1440	0	
	(1 − 2 s) f [Sb1+]	64.66	60.35	0.277	−12.42	64.71	0.0279	−37.71	
	(1 + 2 s) f [Sb1−]	46.11	49.8	0.232	−13.16	46.89	0.0222	−39.76	1.7889×10^{-4}
	Fundamental (f)	50.00	50.1	1.055	0	50.07	2.1599	0	
	(1 − 2 s) f [Sb1+]	53.88	50.39	0.192	−14.76	54.16	0.0192	−41.02	
	(1 + 2 s) f [Sb1−]	36.88	39.06	0.104	−23.9	36.50	0.0327	−36.41	5.2202×10^{-4}
	Fundamental (f)	40.00	40.00	1.641	0	39.96	2.1628	0	
	(1 − s) f [Sb1+]	43.11	40.47	0.196	−18.44	43.64	0.0140	−43.78	
	(1 + 2 s) f [Sb1−]	27.66	29.65	0.285	−12.58	26.78	0.0231	−39.37	6.4835×10^{-4}
	Fundamental (f)	30.00	29.88	1.216	0	29.92	2.1475	0	
	(1 − 2 s) f [Sb1+]	32.33	30.23	0.241	−14.03	33.23	0.0424	−34.09	
	(1 + 2 s) f [Sb1−]	18.44	18.91	0.096	−24.41	18.01	0.0400	−34.41	4.6944×10^{-4}
	Fundamental (f)	20.00	20.00	1.61	0	19.95	2.1011	0	
	(1 − 2 s) f [Sb1+]	21.55	20.63	0.151	−20.52	21.59	0.0277	−37.60	
	(1 + 2 s) f [Sb1−]	9.22	9.21	0.108	−23.1	9.68	0.0305	−36.39	2.4833×10^{-4}
	Fundamental (f)	10.00	10.00	1.543	0	10.05	2.0117	0	
	(1 − 2 s) f [Sb1+]	10.77	11.41	0.071	−26.68	10.60	0.0420	−33.61	

6. Conclusions

It is important to mention that a RCIM should be operating at full load in order to detect BRB_{sbf}, because at full load condition, induced currents circulate at the cage of the rotor and when a measurement of the motor line current is performed, these frequencies will appear; the main difficulty is to extract or detect these BRB_{sbf} because they are frequency components that are too close to the fundamental frequency and some considerations have to be made so that a digital signal processing technique can be used to estimate these frequencies accurately and a diagnostic of the cage of the rotor can be defined. As it is commonly known, FFT analysis is used for RCIM OTD, where this signal processing technique has been used widely in most of online test equipment for RCIM OTD but one of the main disadvantages of the technique for this application is that it requires at least 10 s of recorded signal to give a good estimate of the BRB_{sbf}. Hence, Prony method is proposed to be used as a BRB_{sbf} detection technique to be applied in OTD equipment for RCIM, where at least 25 cycles of a current signal are needed to obtain an accurate estimate of the BRB_{sbf}; with the reduction of a recorded signal with a typical length (10 s), the memory requirement is less in the OTD equipment and the condition of the cage rotor is more accurate. It is important to apply the considerations for Prony method application for RCIM OTD presented in Sections 3 and 4, so an accurate estimate and diagnostic can be achieved.

For future work and recommendations, it is suggested to consider its application and analysis for DC motor current signature. The scope of this work was to present and validate the application details and advantages to use Prony method to determine the condition of

the cage of a RCIM using MCSA. Moreover, it should be mentioned that in comparison with conventional OTD equipment FFT analysis of current signal, Prony method requires at least 25 cycles of recorded data, which means that it leads to a great reduction in memory hardware requirement for the recorded current signal, so an integration of the Prony method in OTD equipment is recommended to increase the accuracy in the condition diagnostic of a cage rotor of a RCIM.

Author Contributions: Conceptualization, methodology, software, validation, resources, data curation, visualization, investigation, writing—original draft preparation, writing—review and editing, L.A.T.G.; software, resources, visualization, investigation, writing—review and editing, M.A.P.G., J.R.M., M.A.G.V., L.H.R.A. and F.S.S. All authors have read and agreed to the published version of the manuscript.

Funding: This research received no external funding.

Institutional Review Board Statement: Not applicable.

Informed Consent Statement: Not applicable.

Data Availability Statement: Not applicable.

Acknowledgments: The authors would like to thank Cuerpo Académico Diagnóstico, Análisis, Control y Medición de Sistemas Eléctricos y Electrónicos (UANL-CA-432) of the Ministry of Public Education of Mexico for allowing us to use the laboratory test system equipment for the corresponding analysis.

Conflicts of Interest: The authors declare no conflict of interest.

Abbreviations

RCIM	Rotor Cage Induction Motor
BRB	Broken Rotor Bar
BRB_{sbf}	Broken Rotor Bar sideband frequencies
Sbf+	Upper sideband frequency
Sbf−	Lower sideband frequency
CBER	Cracked/Broken End Ring
DOL	Direct-On-Line
MCSA	Motor Current Signature Analysis
AAGE	Abnormal Air Gap Eccentricity
OTD	Online Test Diagnostics
MSE	Mean Square Error
VFD	Variable Frequency Drive
FFT	Fast Fourier Transform
DSP	Digital Signal Processing

Appendix A

Table A1. RCIM nameplate data.

Motor Data		
Rated Current	1.98	A
Rated Voltage	208	V
Rated Power	0.5	HP
Temperature insulation class F	155	°C
Rated Frequency	60	Hz
Service factor	1.15	
Efficiency	72	%
Connection	YY	
Rotor cage material	Aluminum	
Rated Speed	1730	RPM

References

1. Singh, G.K.; Kazzaz, S.A.S.A. Induction machine drive condition monitoring and diagnostic research—A survey. *Electr. Power Syst. Res.* **2003**, *64*, 145–158. [CrossRef]
2. Toliyat, H.A.; Nandi, S.; Choi, S.; Meshgin-Kelk, H. *Electric Machines: Modeling, Condition Monitoring, and Fault Diagnosis*, 1st ed.; CRC Press: Boca Raton, FL, USA, 2013.
3. Bonnett, A.H.; Soukup, G.C. Cause and analysis of stator and rotor failures in three-phase squirrel-cage induction motors. *IEEE Trans. Ind. Appl.* **1992**, *28*, 921–937. [CrossRef]
4. Thomson, W.T.; Culbert, I. *Current Signature Analysis for Condition Monitoring of Cage Induction Motors: Industrial Applications and Case Histories*, 1st ed.; John Wiley & Sons, Inc.: Hoboken, NJ, USA, 2017.
5. Messaoudi, M.; Flah, A.; Alotaibi, A.A.; Althobaiti, A.; Sbita, L.; Ziad El-Bayeh, C. Diagnosis and Fault Detection of Rotor Bars in Squirrel Cage Induction Motors Using Combined Park's Vector and Extended Park's Vector Approaches. *Electronics* **2022**, *11*, 380. [CrossRef]
6. Mazouji, R.; Khaloozadeh, H.; Arasteh, M. Fault Diagnosis of Broken Rotor Bars in Induction Motors Using Finite Element Analysis. In Proceedings of the 2020 11th Power Electronics, Drive Systems, and Technologies Conference (PEDSTC), Tehran, Iran, 4–6 February 2020. [CrossRef]
7. Ferrucho-Alvarez, E.R.; Martinez-Herrera, A.L.; Cabal-Yepez, E.; Rodriguez-Donate, C.; Lopez-Ramirez, M.; Mata-Chavez, R.I. Broken Rotor Bar Detection in Induction Motors through Contrast Estimation. *Sensors* **2021**, *21*, 7446. [CrossRef] [PubMed]
8. Drakaki, M.; Karnavas, Y.L.; Karlis, D.A.; Chasiotis, I.D.; Tzionas, P. Study on fault diagnosis of broken rotor bars in squirrel cage induction motors: A multi-agent system approach using intelligent classifiers. *Inst. Eng. Technol.* **2020**, *14*, 245–255. [CrossRef]
9. Bazan, G.H.; Goedtel, A.; Duque-Perez, O.; Morinigo-Sotelo, D. Multi-Fault Diagnosis in Three-Phase Induction Motors Using Data Optimization and Machine Learning Techniques. *Electronics* **2021**, *10*, 1462. [CrossRef]
10. Martinez-Herrera, A.L.; Ferrucho-Alvarez, E.R.; Ledesma-Carrillo, L.M.; Mata-Chavez, R.I.; Lopez-Ramirez, M.; Cabal-Yepez, E. Multiple Fault Detection in Induction Motors through Homogeneity and Kurtosis Computation. *Energies* **2022**, *15*, 1541. [CrossRef]
11. Liu, X.; Yan, Y.; Hu, K.; Zhang, S.; Li, H.; Zhang, Z.; Shi, T. Fault Diagnosis of Rotor Broken Bar in Induction Motor Based on Successive Variational Mode Decomposition. *Energies* **2022**, *15*, 1196. [CrossRef]
12. Bonet-Jara, J.; Morinigo-Sotelo, D.; Duque-Perez, O.; Serrano-Iribarnegaray, L.; Pons-Llinares, J. End-ring wear in deep well submersible motor pumps. In Proceedings of the IEEE Transactions on Industry Applications, Greenfield, WI, USA, 12 April 2022. [CrossRef]
13. Elvira-Ortiz, D.A.; Morinigo-Sotelo, D.; Zorita-Lamadrid, A.L.; Osornio-Rios, R.A.; Romero-Troncoso, R.d.J. Fundamental Frequency Suppression for the Detection of Broken Bar in Induction Motors at Low Slip and Frequency. *Appl. Sci.* **2020**, *10*, 4160. [CrossRef]
14. Zamudio-Ramirez, R.A.; Osornio-Rios, J.A.; Antonino-Daviu, H.R.; Romero-Troncoso, R.d.J. Magnetic Flux Analysis for the Condition Monitoring of Electric Machines: A Review. In Proceedings of the IEEE Transactions on Industry Applications, Taipei, Taiwan, 2 April 2022; Volume 18, pp. 2895–2908. [CrossRef]
15. Garcia-Calva, T.A.; Morinigo-Sotelo, D.; Romero-Troncoso, R.D.J. Fundamental Frequency Normalization for Reliable Detection of Rotor and Load Defects in VSD-fed Induction Motors. In Proceedings of the IEEE Transactions on Industry Applications, Trieste, Italy, 13 November 2021. [CrossRef]
16. Fernandez-Cavero, V.; Pons-Llinares, J.; Duque-Perez, O.; Morinigo-Sotelo, D. Detection of Broken Rotor Bars in Nonlinear Startups of Inverter-Fed Induction Motors. In Proceedings of the IEEE Transactions on Industry Applications, Greenfield, WI, USA, 17 March 2021; Volume 57, pp. 2559–2568. [CrossRef]
17. Fernandez-Cavero, V.; Pons-Llinares, J.; Duque-Perez, O.; Morinigo-Sotelo, D. Detection and quantification of bar breakage harmonics evolutions in inverter-fed motors through the dragon transform. *ISA Trans.* **2021**, *109*, 352–367. [CrossRef]
18. Fernandez-Cavero, V.; García-Escudero, L.A.; Pons-Llinares, J.; Fernández-Temprano, M.A.; Duque-Perez, O.; Morinigo-Sotelo, D. Diagnosis of Broken Rotor Bars during the Startup of Inverter-Fed Induction Motors Using the Dragon Transform and Functional ANOVA. *Appl. Sci.* **2021**, *11*, 3769. [CrossRef]
19. Garcia-Calva, T.A.; Morinigo-Sotelo, D.; Fernandez-Cavero, V.; Garcia-Perez, A.; Romero-Troncoso, R.d.J. Early Detection of Broken Rotor Bars in Inverter-Fed Induction Motors Using Speed Analysis of Startup Transients. *Energies* **2021**, *14*, 1469. [CrossRef]
20. Pezzani, C.; Donolo, P.; Bossio, G.; Donolo, M.; Guzmán, A.; Zocholl, S.E. Detecting Broken Rotor Bars With Zero-Setting Protection. In Proceedings of the IEEE Transactions on Industry Applications, Greenfield, WI, USA, 31 July 2014; Volume 50, pp. 1373–1384. [CrossRef]
21. Ayhan, B.; Chow, M.-Y.; Trussell, H.J.; Song, M.-H. A case study on the comparison of non-parametric spectrum methods for broken rotor bar fault detection. In Proceedings of the 29th Annual Conference of the IEEE Industrial Electronics Society (IECON), Roanoke, VA, USA, 2–6 November 2003. [CrossRef]
22. Ribeiro, P.F.; Duque, C.A.; Ribeiro, P.M.; Cerqueira, A.S. *Power Systems Signal Processing for Smart Grids*, 1st ed.; Wiley: London, UK, 2014.
23. Trujillo-Guajardo, L.A.; Rodriguez-Maldonado, J.; Moonem, M.A.; Platas-Garza, M.A. A Multiresolution Taylor–Kalman Approach for Broken Rotor Bar Detection in Cage Induction Motors. *IEEE Trans. Inst. Meas.* **2018**, *67*, 1317–1328. [CrossRef]

24. Naha, A.; Samanta, A.K.; Routray, A.; Deb, A.K. A method for detecting half-broken rotor bar in lightly loaded induction motors using current. *IEEE Trans. Inst. Meas.* **2016**, *65*, 1614–1625. [CrossRef]
25. Valles-Novo, R.; Rangel-Magdaleno, J.; Ramirez-Cortes, J.M.; Peregrina-Barreto, H.; Morales-Caporal, R. Empirical mode decomposition analysis for broken-bar detection on squirrel cage induction motors. *IEEE Trans. Inst. Meas.* **2015**, *64*, 1118–1128. [CrossRef]
26. Picazo-Rdenas, M.J.; Antonino-Daviu, J.; Climente-Alarcon, V.; Royo-Pastor, R.; Mota-Villar, A. Combination of noninvasive approaches for general assessment of induction motors. *IEEE Trans. Ind. Appl.* **2015**, *51*, 2172–2180. [CrossRef]
27. Wang, J.; Gao, R.X.; Yan, R. Broken-Rotor-Bar Diagnosis for Induction Motors. In Proceedings of the 9th International Conference on Damage Assessment of Structures (DAMAS 2011), London, UK, 11–13 July 2011.
28. Bessam, B.; Menacer, A.; Boumehraz, M.; Cherif, H. Detection of broken rotor bar faults in induction motor at low load using neural network. *ISA Trans.* **2016**, *64*, 241–246. [CrossRef]
29. Sahraoui, M.; Cardoso, A.J.M.; Ghoggal, A. The Use of a Modified Prony Method to Track the Broken Rotor Bar Characteristic Frequencies and Amplitudes in Three-Phase Induction Motors. *IEEE Trans. Ind. Appl.* **2014**, *51*, 2136–2147. [CrossRef]
30. Jia, Z.; Zhu, H.; Liu, X.; Shang, H. Incipient Broken Rotor Bar Fault Diagnosis Based on Extended Prony Spectral Analysis Technique. In Proceedings of the 2018 37th Chinese Control Conference (CCC), Wuhan, China, 25–27 July 2018. [CrossRef]
31. Chen, S.; Zivanovic, R. Estimation of frequency components in stator current for the detection of broken rotor bars in induction machines. *Measurement* **2010**, *43*, 887–900. [CrossRef]
32. Xu, B.Q.; Tian, S.H. *A Detection Method for Broken Rotor Bar Fault in Induction Motors Based on SVD Combined MUSIC with Extended Prony*; Applied Mechanics and Materials Trans Tech Publications, Ltd.: Basel, Switzerland, 2014; Volume 707, pp. 333–337. [CrossRef]
33. Dehina, W.; Boumehraz, M.; Kratz, F. On-line detection and estimation of harmonics components in induction motors rotor fault through a modified Prony's method. *Int. Trans. Electr. Energ. Syst.* **2021**, *31*. [CrossRef]
34. Lobos, T.; Rezmer, J.; Schegner, J. Parameter estimation of distorted signals using Prony method. In Proceedings of the 2003 IEEE Bologna Power Tech Conference Proceedings, Bologna, Italy, 23–26 June 2003. [CrossRef]
35. Leonowicz, Z.; Lobos, T.; Rezmer, J. Advanced Spectrum Estimation Methods for Signal Analysis in Power Electronics. *IEEE Trans. Ind. Electr.* **2003**, *50*, 514–519. [CrossRef]
36. Wrocław University of Science and Technology Digital Library. Parametric Methods for Time–Frequency Analysis of Electric Signals. Available online: https://www.dbc.wroc.pl/dlibra/publication/1877/edition/2021?language=pl (accessed on 15 February 2022).
37. Qi, L.; Qian, L.; Woodruff, S.; Cartes, D. Prony Analysis for Power System Transients. *EURASIP J. Adv. Signal Processing* **2007**, *2007*, 048406. [CrossRef]
38. Meunier, M.; Brouaye, F. Fourier transform, Wavelets, Prony Analysis: Tools for Harmonics and Quality of Power. In Proceedings of the 8th Int. Conf. on Harmonics and Quality of Power ICHQP'98, Athens, Greece, 14–16 October 1998. [CrossRef]
39. Johnson, M.A.; Zarafonitis, I.P.; Calligaris, M. Prony analysis and power system stability-some recent theoretical and applications research. In Proceedings of the 2000 Power Engineering Society Summer Meeting, Seattle, WA, USA, 16–20 July 2000. [CrossRef]
40. Castillo, R.; Ramírez, J.R.; Alonso, G.; Ortiz-Villafuerte, J. Prony's method application for BWR instabilities characterization. *Nucl. Eng. Des. J.* **2014**, *284*, 67–73. [CrossRef]
41. Trujillo Guajardo, L.A. Relevador De Protección De Distancia Con Estimador Fasorial De Prony (MX Patent No. 351620 B). México Patent Office, Instituto Mexicano de la Propiedad Industrial, IMPI. 2017. Available online: https://vidoc.impi.gob.mx/visor?usr=SIGA&texp=SI&tdoc=E&id=MX/a/2014/012486 (accessed on 12 January 2022).
42. Trujillo Guajardo, L.A. Prony filter vs conventional filters for distance protection relays: An evaluation. *Electr. Power Syst. Res.* **2016**, *137*, 163–174. [CrossRef]